Absolute Intensities for Third and Fourth Overtone Absorptions in HNO_3 and H_2O_2 Measured by Cavity Ring Down Spectroscopy

Steven S. Brown,[†] Robert W. Wilson, and A. R. Ravishankara*[,‡]

National Oceanic and Atmospheric Administration, Aeronomy Laboratory, R/AL2, 325 Broadway, Boulder, Colorado 80303

Received: February 3, 2000; In Final Form: March 17, 2000

Photodissociation of nitric acid and hydrogen peroxide via high-lying O−H overtone absorptions in the visible may act as a source of OH radicals in the atmosphere. We have used cavity ring down spectroscopy to measure the absorption cross sections for the third ($4\nu_{OH}$) and fourth ($5\nu_{OH}$) overtone transitions in these molecules. The integrated cross sections are $(2.25 \pm 0.15) \times 10^{-21}$ and $(2.57 \pm 0.24) \times 10^{-22}$ cm^2 molecule^{-1} cm^{-1} for $4\nu_{OH}$ and $5\nu_{OH}$ in nitric acid, respectively, and $(4.58 \pm 0.39) \times 10^{-21}$ and $(5.67 \pm 0.52) \times 10^{-22}$ cm^2 molecule^{-1} cm^{-1} for $4\nu_{OH}$ and $5\nu_{OH}$ in hydrogen peroxide. For both molecules, our report is the first direct intensity measurement for $5\nu_{OH}$, the lowest dissociative overtone transition. We compare our values for the lower overtones to those from previous studies, where available. Our measured cross sections suggest that the contribution of direct overtone excitation to the atmospheric photodissociation of HNO_3 and H_2O_2 is small but not completely negligible.

Introduction

Odd hydrogen species (HO_x = OH and HO_2) are present in the stratosphere and troposphere primarily as a result of ozone photolysis and the subsequent reaction of $O(^1D)$ with water.[1] Smaller contributions arise from various sources such as acetone degradation[2,3] and bromine nitrate hydrolysis followed by photolysis of the HOBr product.[4−6] Recent comparisons of calculated and observed HO_x abundances in the lower stratosphere have shown that there is a burst of HO_x at sunrise.[7,8] The bromine chemistry mentioned above is responsible for part but not all of the observed HO_x behavior.[9] Thus, the observations imply an unknown source of HO_x radicals. One component of this source may be the photolysis of OH containing compounds in the visible via transitions to O−H stretch overtone states that lie near or above the threshold for dissociation of one of the other bonds in the molecule.[10] This mechanism is known as direct overtone photolysis, DOP, and candidate molecules include nitric acid (HNO_3), hydrogen peroxide (H_2O_2), and pernitric acid (HO_2NO_2). Thus, atmospheric photodissociation of OH containing molecules via direct overtone excitation of the O−H chromophore has been a topic of recent interest.[11,12]

Donaldson et al.[10] presented a calculation of the enhancement in the atmospheric photodissociation rates of H_2O_2, HNO_3, and HO_2NO_2 due to DOP. These authors estimated the absorption cross sections for the very weak overtone transitions that could lead to dissociation: five or more quanta of O−H stretch ($5\nu_{OH}$) in both $HONO_2$ and H_2O_2 and three or more quanta in HO_2NO_2. In making absorption cross section estimates, these authors used the rule of thumb given by Crim[13] that the intensity of successive overtones is smaller by a factor of 10. Recently, Donaldson et al.[11] measured overtone intensities in nitric acid up to $4\nu_{OH}$ and presented an ab initio calculation of the intensities of higher, dissociative overtones. However, because the dissociative fourth overtone ($5\nu_{OH}$) is weak (peak intensities of $<10^{-23}$ cm^2 molecule^{-1}), and because there is significant interference near the 618 nm $5\nu_{OH}$ transition due to absorption by NO_2 that is inevitably present in nitric acid samples, these authors were unable to measure this cross section directly. While our work was in progress, we also became aware of the study by Zhang et al.,[14] who have measured second and third overtone cross sections for HNO_3 and H_2O_2, as well as HO_2NO_2, using long-path absorption. We are unaware of any other direct measurements of the overtone intensities in H_2O_2 and HNO_3 that lead to dissociation and that are, therefore, needed for calculation of atmospheric photolysis rates.

Cavity ring down spectroscopy (CRDS) is a recently developed technique for measuring weak molecular absorption.[15] It is ideally suited to determination of absolute overtone intensities; indeed, Lehmann and co-workers have demonstrated observations of strongly forbidden transitions up to eight quanta of C−H stretch in HCN.[16] Although CRDS is relatively novel, it has seen increasing use in the last several years.[17,18] Briefly, the technique measures the loss rate of light out of an optical cavity formed by two highly reflective mirrors. In the empty cavity, the finite transmission of light through the mirrors determines the loss rate. The presence of an absorbing gas inside of the cavity introduces an additional loss, and the difference in the first-order loss rate coefficient of the empty cavity relative to that of the cavity plus absorber provides a sensitive measure of the absorbance (the product of the absorber's number density and absorption cross section).

We present the first experimental measurements of the absolute absorption cross sections for the $5\nu_{OH}$ transition in both nitric acid and hydrogen peroxide, as well as overtone intensities for the $4\nu_{OH}$ transitions in both of these species. The CRDS measurements provide somewhat better signal-to-noise than previous measurements of $4\nu_{OH}$ transitions and better resolution of the rotational band structure. In addition to the absolute intensities, we have measured the rotational profiles for $4\nu_{OH}$

* To whom correspondence should be addressed.
[†] NOAA NRC Postdoctoral Fellow.
[‡] Also affiliated with the Department of Chemistry and Biochemistry, University of Colorado, Boulder, CO 80309.

10.1021/jp000439d
Published on Web 05/04/2000

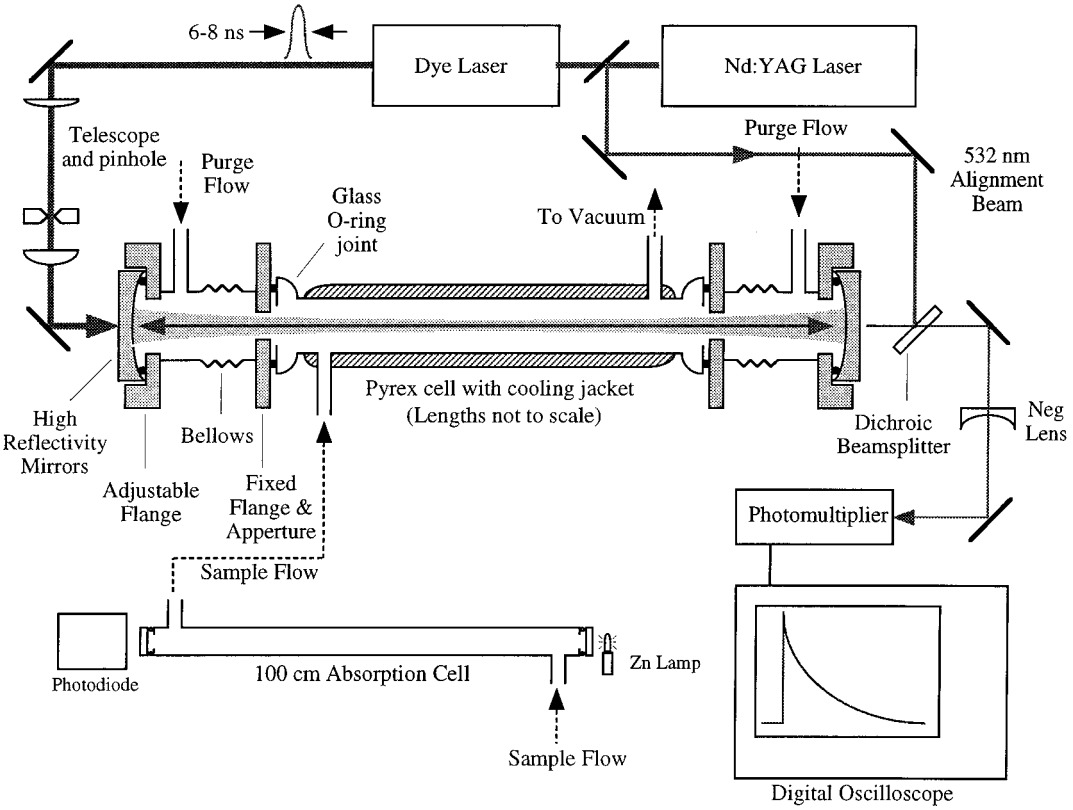

Figure 1. Experimental apparatus.

and $5\nu_{OH}$ in HNO_3 and for $4\nu_{OH}$ in H_2O_2 at two different temperatures, 296 and 251−253 K, the latter of which is more relevant in the mid to upper troposphere.

Experimental Section

Figure 1 is a schematic of the cavity ring down apparatus. The light source was a Nd:YAG laser pumped dye laser with a pulse duration of 6−8 ns (manufacturers specification) and a bandwidth of approximately 0.06−0.08 cm^{-1} depending on the wavelength. We measured the bandwidth by scanning individual rotational lines in the overtone spectrum of water and in the (b $^1\Sigma^+ \leftarrow X\ ^3\Sigma^-$) spectrum of O_2. These bands also served as a convenient calibration for the dye laser wavelength. We attenuated the dye laser output energy to approximately 10−20 mJ/pulse by either blocking the preamplifier stage and/or placing a neutral density filter at the output. The output beam propagated through an aperture, a series of turning prisms, and a 5:1 telescope with either a 50 or 100 μm pinhole at the focus to spatially filter the beam. The telescope and filter served to more closely match the input beam to the TEM_{00} modes of the optical cavity, which had a calculated diameter of slightly less than 1 mm at the cavity mirrors. The beam impinged directly along the cavity axis on one of the end mirrors, which transmitted a small fraction ($(1-3) \times 10^{-5}$) of the incoming light.

The light leaking out the opposite end of the cavity propagated through two turning prisms, a negative lens, and a sharp cutoff, color glass filter that eliminated shorter wavelength scattered room light, before striking a red-sensitive photomultiplier tube (PMT). A digital oscilloscope captured, digitized, and averaged the PMT output, and the temporal intensity profile was transferred to a lab computer. A black aluminum box with a variable aperture for the input beam covered all of the signal collection optics and minimized stray light at the photomultiplier. We split off a small fraction of the 532 nm Nd:YAG second harmonic beam with a quartz plate prior to the dye laser. The 532 nm beam, aligned on the cavity axis, was transmitted by the cavity mirrors and was very useful for cavity alignment.

The computer was interfaced to the digital scope such that the captured waveform was analyzed to obtain the ring down time. The averaged waveform was transformed to a log-(intensity) vs time profile and fit to a line using a linear least squares algorithm. The resulting slope was the inverse of the time constant for the single-exponential decay of light intensity from the cavity. Since the digital scope had 8-bit resolution, averaging multiple profiles reduced the digital noise, although we could not obtain useful decays beyond a factor of ∼50 decrease from the maximum intensity. The computer also controlled a stepping motor that tuned the dye laser grating and thus its wavelength. To acquire a spectrum, the computer stepped the grating between acquisition of ring down profiles and produced a plot of the ring down time constant as a function of the dye laser wavelength. Acquisition of the spectrum of an absorber with known, discrete rotational lines, such as that of O_2 or water overtones, allowed calibration of the dye laser wavelength.

The high-reflectivity cavity mirrors had a 1 m radius of curvature and a separation of approximately 95 cm. The maximum observed empty cavity ring down times were 240 μs at 760 nm and 120 μs at 633 nm, the two wavelengths of peak reflectivity for each set of mirrors. In practice, the empty cavity ring down times were generally somewhat shorter, due both to the variation in decay time with wavelength and presumably also to imperfectly clean mirrors. Each mirror mount consisted of an adjustable flange connected to a fixed flange by a flexible bellow, similar to the apparatus of Atkinson et al.[19] Commercial kinematic mirror mounts holding the adjustable flanges and mirrors allowed for cavity mirror alignment while still maintain-

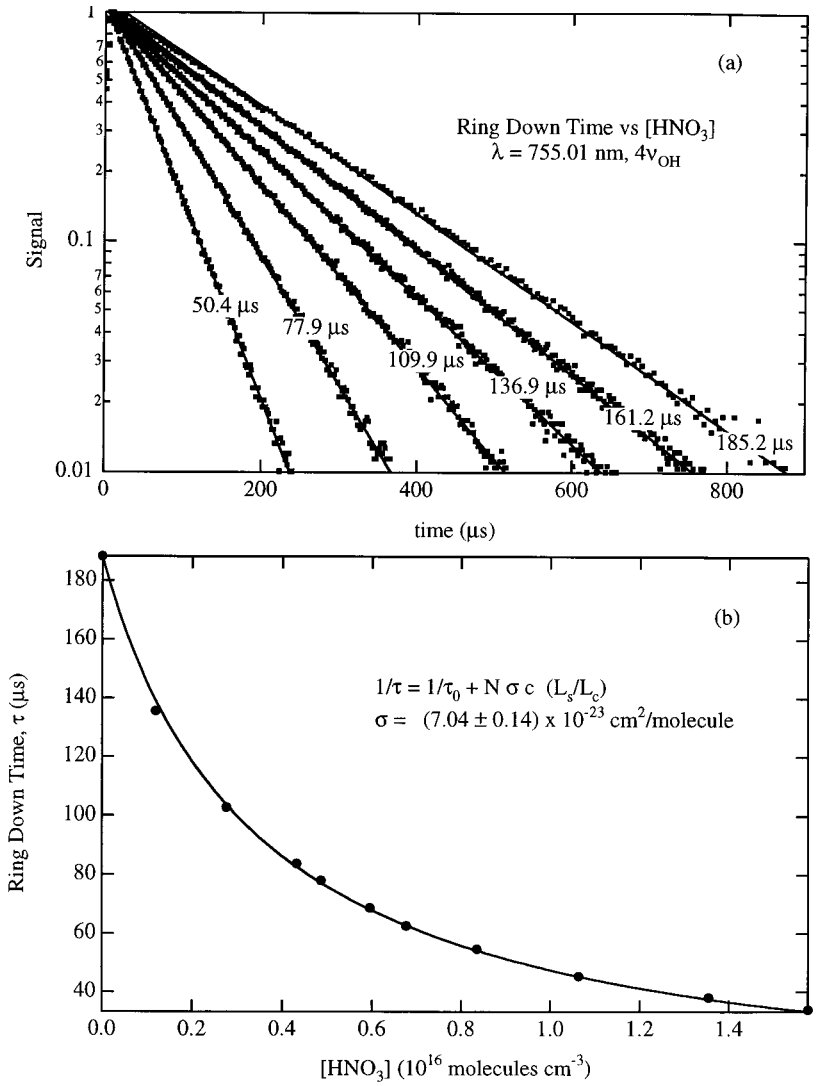

Figure 2. (a) Series of exponential decays with the laser tuned to the peak of the HNO_3 $4\nu_{OH}$ Q branch transition at 755.01 nm. (b) Plot of measured ring down time vs HNO_3 concentration (points) and a fit to eq 1 (solid line). Note that the points in (b) do not correspond to the ring down traces shown in (a).

ing a vacuum seal. A small flow of purge gas introduced into the volume between the adjustable and fixed flanges ensured that potentially condensable or corrosive gases inside the main cavity volume did not come into contact with the mirrors. A small stainless steel aperture ($^1/_8$ or $^1/_4$ in. diameter) mounted between the purge volume and the main cavity increased the linear flow velocity between the volumes and minimized flow back into the purge volume. The apertures also helped to better define the cavity length over which the sample gas was present (see below). The mirror cleanliness, as measured by the empty cavity ring down time, remained essentially unchanged over the course of several weeks of experiments using this arrangement.

The main volume of the cavity consisted of a jacketed, Pyrex cell of approximately $^3/_4$ in. inner diameter, with glass O-ring joints to seal to the fixed flanges/apertures of the purge volumes. Sample and carrier gases flowed from one end of this volume and out the other end. Silicone oil or methanol coolant from a temperature-controlled bath circulated through the outer jacket to regulate the temperature of the gas inside. The gas flow entered the cell axis through a short, jacketed region in order to precool it. Thermocouples inserted almost to the center of the cell near both ends measured the gas temperature, which varied by less than ± 1 K over the cell length. Helium was the carrier/purge gas for all experiments, and the total cell pressure varied between 20 and 100 Torr. Because the $4\nu_{OH}$ and $5\nu_{OH}$ transitions in both HNO_3 and H_2O_2 are relatively broad and rotationally congested, there was no discernible effect on line shapes due to changes in buffer gas pressure. The mirror alignment was also not sensitive to the internal cell pressure over this range. A small, adjustable flow of He gas flowed through a bubbler containing either liquid HNO_3 (anhydrous) or H_2O_2 (>90%) and mixed with the main gas flow just prior to entering the cell. We measured all gas flows using calibrated, electronic mass flow meters.

We measured the concentrations of HNO_3 and H_2O_2 vapor via absorption of the 213.86 nm Zn line in a 100 cm absorption cell located either just upstream or just downstream from the ring down cell. We used absorption cross sections of $(4.52 \pm 0.19) \times 10^{-23}$ [20,21] and $(3.30 \pm 0.22) \times 10^{-23}$ cm^2 [22] to calculate HNO_3 and H_2O_2 concentrations, respectively. Typical gas-phase concentrations of either absorber were $(1-3) \times 10^{16}$ molecules cm^{-3} except for H_2O_2 at 250 K, where the vapor pressure limited the maximum concentration to $<10^{15}$ molecules cm^{-3}. For this reason we did not scan the $5\nu_{OH}$ spectrum of H_2O_2 at 250 K. When using H_2O_2, it was convenient to place the absorption cell upstream of the ring down cell. For measurement of the $5\nu_{OH}$ intensity in HNO_3 the absorption cell was located

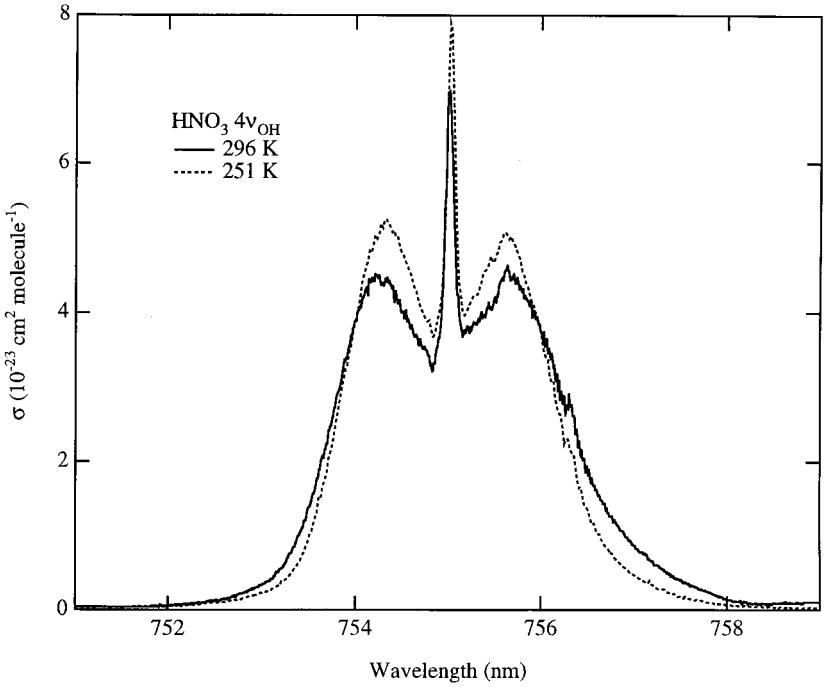

Figure 3. Third O−H stretch overtone ($4\nu_{OH}$) spectrum of nitric acid at two different temperatures, 296 K (solid line) and 251 K (dashed line). The abscissa in this and all subsequent spectra is vacuum wavelength.

downstream from the ring down cell to minimize the formation of NO_2 on surfaces prior to the ring down measurement. Nitrogen dioxide has an absorption cross section nearly 4 orders of magnitude larger than HNO_3 at 618 nm,[23] and thus even small contamination by NO_2 strongly affected the signal at this wavelength. We synthesized HNO_3 from the dropwise addition of concentrated sulfuric acid to solid sodium nitrate under vacuum and collected the evolving HNO_3 vapor in a trap at 77 K. Addition of a small amount of water to the anhydrous sample suppressed the formation of N_2O_5, whose presence can give rise to a strong absorption signal from its gas-phase decomposition product, NO_3, near the $5\nu_{OH}$ transition in HNO_3. We concentrated 70% H_2O_2 by distilling it into vacuum for a period of several days prior to use. We measured its purity to be greater than 95% (by weight) by titration with $KMnO_4$.

Results and Data Analysis

Figure 2a displays a series of decays (logarithmic scale) at different absorber concentrations (HNO_3 near 755 nm) along with single-exponential fits ($e^{-t/\tau}$) to the data. (Here t is the time and τ is the time constant for the ring down.) The traces are the result of 64 averages. The largest source of noise in these traces came from the 8 bit signal digitization. The traces in Figure 2 have been averaged such that this digitization noise is partially removed.

There is an inverse relationship between the sample absorbance, α, and the observed ring down time.[24]

$$\alpha(\mathrm{cm}^{-1}) = N\sigma(\omega) = \frac{1}{c}\frac{L}{L_s}\left(\frac{1}{\tau} - \frac{1}{\tau_0}\right) \qquad (1)$$

Here N is the number density of absorbers, $\sigma(\omega)$ is the frequency dependent absorption cross section, c is the speed of light, L is the total cavity length, L_S is the length over which sample is present, τ is the observed ring down time in the presence of the absorber, and τ_0 is the ring down time in the empty cavity. The minimum detectable absorbance depends on both τ_0 and the precision with which τ can be measured.

$$\alpha_{min} = \frac{1}{c}\frac{L}{L_S}\frac{\Delta t_{min}}{\tau_0}\frac{1}{\tau_0} \qquad (2)$$

Here Δt_{min} is the smallest observable change in τ, or in other words, the uncertainty in τ_0. Thus, the ratio $\Delta t_{min}/\tau_0$ is the fractional uncertainty in τ_0. For a typical τ_0 fractional uncertainty of 0.5% and a τ_0 of 200 μs, α_{min} is on the order of 10^{-9} cm^{-1}.

We determined the factor of L/L_S in eq 1 empirically by measuring the absorbance of O_3 in the Chappius bands. We introduced a flow of O_3 into the apparatus and measured its concentration via UV absorption at either 213.86 nm (Zn lamp) or at 253.65 nm (Hg lamp).[25] The absorption cross sections for the Chappius bands are well-known.[26] The L/L_S ratio was obtained from the ratio of the literature cross sections to the cross sections determined from eq 1 without the factor of L/L_S. We found $L/L_S = 1.34 \pm 0.06$ over the range of different main gas/purge volume flow rates used in these experiments. This ratio agreed with the measured geometric ratio of the total cell length to the length of the main cell body. Figure 2b is a plot of ring down time vs HNO_3 concentration at the wavelength of the peak observed cross section in the $4\nu_{OH}$ band (755.01 nm; see Figure 3). The points are the observed ring down times and the solid line is a fit to eq 1, with σ as the fit parameter. The observed time constants follow eq 1 to within 2% (uncertainty in the fit).

Figures3−6 are plots of absolute absorption cross sections for the $4\nu_{OH}$ and $5\nu_{OH}$ transitions in HNO_3 and H_2O_2 at two different temperatures. To obtain these data, we first coarsely scanned (0.5 nm/step) the spectrum of the empty cavity to record the variation in ring down time with wavelength and then fit this variation to a smooth function, typically a third-order polynomial. We then introduced the absorbing sample and monitored its concentration while finely scanning (0.005−0.01 nm/step) the dependence of ring down time on wavelength. We typically averaged 16−32 shots for each ring down decay. Use of eq 1 with the known concentrations gave absolute absorption intensities. Immediately prior to or after each scan, we scanned either the overtone spectrum of water vapor or the absorption

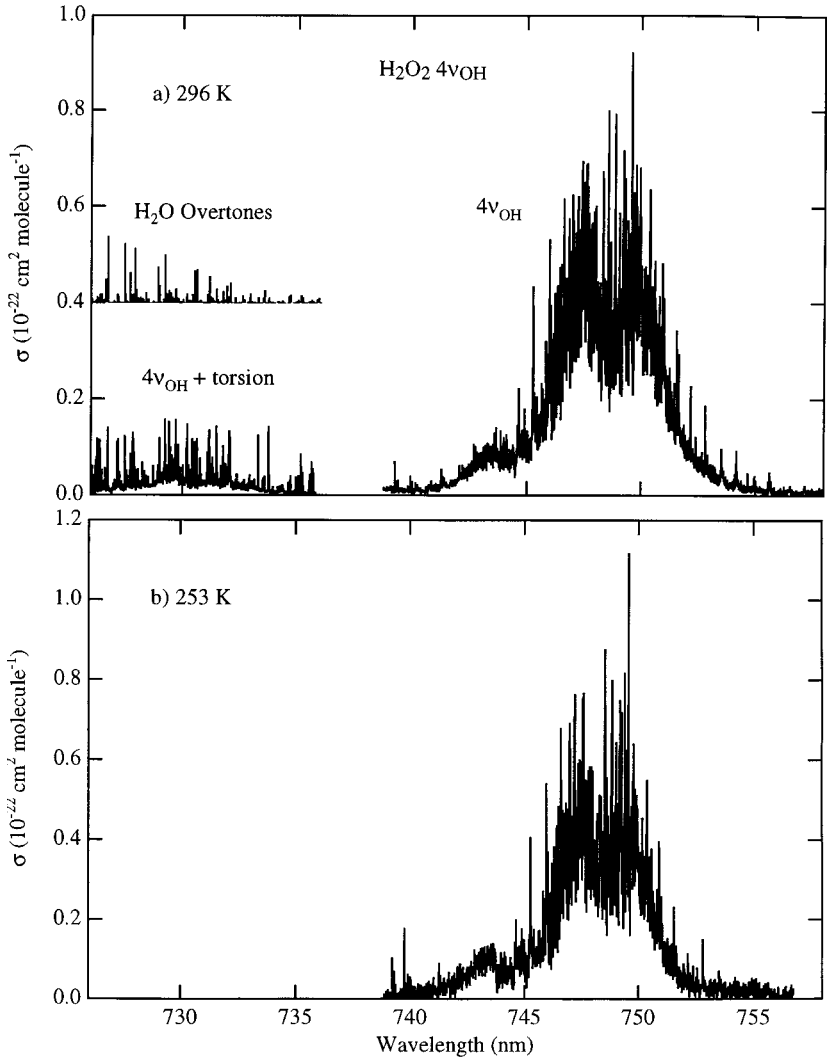

Figure 4. Third O−H stretch overtone ($4\nu_{OH}$) spectrum of hydrogen peroxide at (a) 296 K and (b) 253 K. The band consists of the $4\nu_{OH}$ transition and a weaker band that is $4\nu_{OH}$ plus a quantum of the torsional vibration. The sharp structure over the weak combination band is due to interference from water overtones. The overlay above this part of the spectrum is a stick spectrum for H_2O. The water spectrum is transparent in the region of the strong absorption.

spectrum of O_2 (as noted above) to give a wavelength calibration.[27] The vacuum wavelength scale in Figures 3−6 is accurate to within ±0.01 nm, the limit of the variability in the dye laser wavelength upon successive scans of the same spectrum.

The nitric acid spectra show only very broad features, while the H_2O_2 spectra showed somewhat more rotational structure, although the majority of the absorption was due to a broad underlying continuum. This was particularly true for the $5\nu_{OH}$ band. The strongest sharp features in the $4\nu_{OH}$ spectrum of H_2O_2 have line widths of 0.3−0.4 cm^{-1}, several times larger than the dye laser bandwidth. This is an important criterion since an absorption feature with a width approaching that of the laser bandwidth gives rise to a multiexponential temporal profile. (The departure from a single exponential decay arises if different wavelengths underneath the laser bandwidth have different loss rates inside the cavity, as they do if the absorption line profile varies rapidly over the laser bandwidth).[24] CRDS traces appeared to be exponential at all wavelengths in the H_2O_2 absorption band. (By contrast, nonexponential decays were observed for strong absorptions in the water overtone or O_2 absorption calibration spectra, where the Doppler/pressure broadened line widths are equal to or narrower than the dye laser bandwidth.)

The two important interfering absorbers were H_2O overtones in the $4\nu_{OH}$ spectrum of H_2O_2 and NO_2 absorption in the $5\nu_{OH}$ spectrum of HNO_3. The interfering water lines are present only over the very weak transitions at the short wavelength side of the H_2O_2 absorption. A stick spectrum of H_2O overtones[27] appears as an overlay above the data on the right side of Figure 4a. The intensity pattern of the water overtones in the stick spectrum does not exactly match the sharp lines in the data because of errors arising from the narrow line width of H_2O overtones, as discussed above. However, the frequency pattern of the sharp lines in the data verifies that they belong to H_2O. Only the weak, underlying broad structure on the right side of Figure 4a comes from H_2O_2 absorption. Even when highly concentrated liquid H_2O_2 samples (>95%) were used, a significant amount of water was present in the vapor, and the lines in the third overtone of water vapor have large peak absorption cross sections compared to H_2O_2. Therefore, to measure the integrated intensity of the weak band in the H_2O_2 spectrum we subtracted the sharp features due to H_2O from the broad, underlying continuum due to H_2O_2. This procedure introduced some uncertainty into the measured values as described below. The main overtone absorption band in H_2O_2 (and in HNO_3) lies in a wavelength region where water does not absorb.[27] The overlap of water lines with the weak band in the $5\nu_{OH}$ band (Figure 6) of H_2O_2 is less severe.

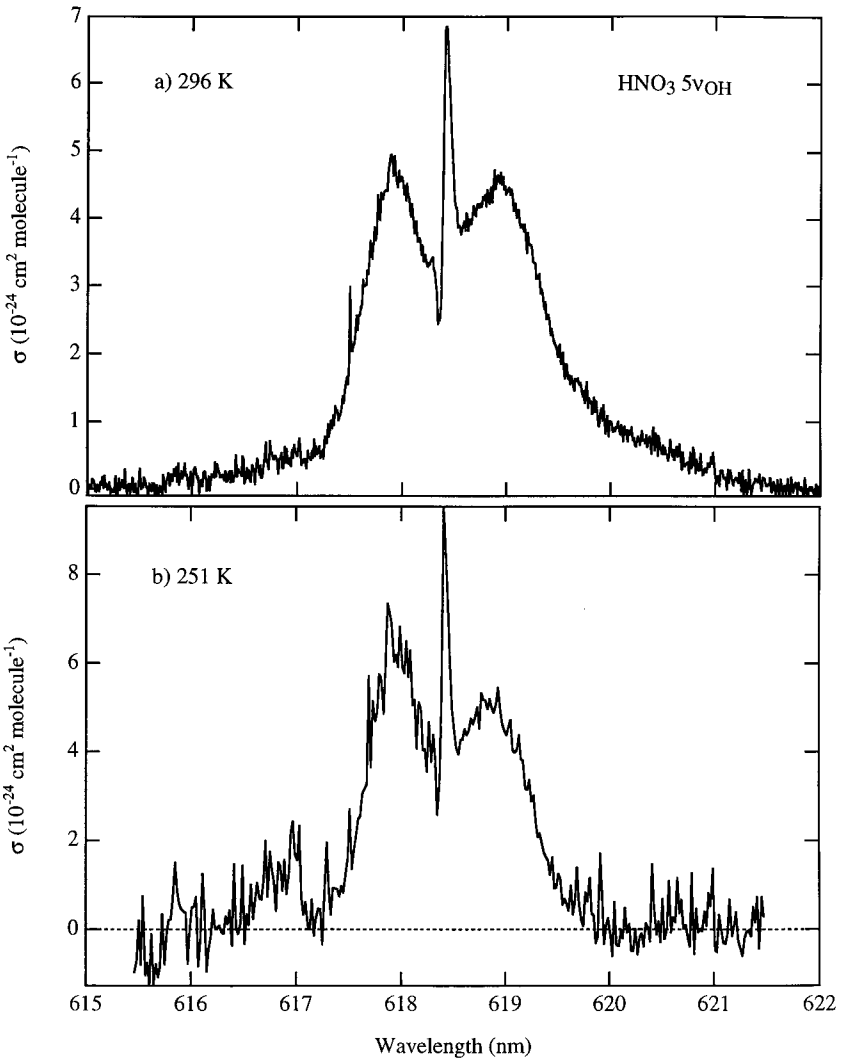

Figure 5. Fourth O−H stretch overtone ($5\nu_{OH}$) spectrum of nitric acid at (a) 296 K and (b) 251 K. The noise on the baseline in both plots arises primarily from NO_2 absorption, which has been subtracted.

The $5\nu_{OH}$ band of HNO_3 has a somewhat more serious interference from NO_2 absorption since NO_2 is unavoidably present in nitric acid samples. Introduction of the nitric acid sample directly from the bubbler to the ring down cell along with increasing the linear flow velocity through the cell minimized the observed absorption due to NO_2. We achieved maximum HNO_3 ($5\nu_{OH}$)/NO_2 absorption signals of approximately 10:1, corresponding to a fractional NO_2 contamination of $(1-2) \times 10^{-5}$ in HNO_3. This level of NO_2 impurity in HNO_3 is consistent with our previous observations.[21] We subtracted the NO_2 absorption from the HNO_3 signal by averaging the baseline on either side of the $5\nu_{OH}$ band and subtracting this average value from the spectrum. This procedure did not accurately subtract out the structure in the NO_2 absorption, as can be seen by the noisy baseline on the HNO_3 band, particularly on the low-temperature spectrum in Figure 5b. Since the NO_2 absorption was quite weak, however, the structure was not easily discernible and would have been difficult to subtract accurately. Since there is less than a factor of 2 variation in the NO_2 cross section over this spectral range,[23] the subtraction procedure should lead to no more than a ±5% error in the measured cross sections at room temperature (Figure 5a) and ±13% at low temperature (Figure 5b).

Discussion

Rotational Structure. The rotational contours of the nitric acid overtones, as noted above, are broad, showing no discernible structure other than smoothly varying envelopes of the P and R branches and a sharper Q branch. Sinha et al.[28] suggest that this smooth spectrum is due primarily to rotational congestion. The lack of rotational resolution does not allow comparison of vibrationally excited-state lifetimes between the $4\nu_{OH}$ band, which lies well below the threshold for dissociation to OH + NO_2, and the $5\nu_{OH}$ band, which contains transitions to rovibrational states lying just above threshold. There is an obvious change in the $4\nu_{OH}$ and $5\nu_{OH}$ rotational contours with temperature (Figures 3 and 5). As one might expect, the P and R branch envelopes narrow measurably at lower temperatures due to depopulation of higher lying rotational states. The band narrowing at lower temperature is not likely to have any significant effect on the atmospheric absorption rate via the $5\nu_{OH}$ state unless the solar flux varies significantly over the narrow wavelength range of the band due to, for example, Fraunhaufer lines in the solar spectrum or overhead absorption by other species such as oxygen or water. Fraunhaufer lines are quite dense in the region near 618 nm and are likely to affect the absorption in the high or low-temperature rotational profiles about equally. The $5\nu_{OH}$ transition lies in a region of the water

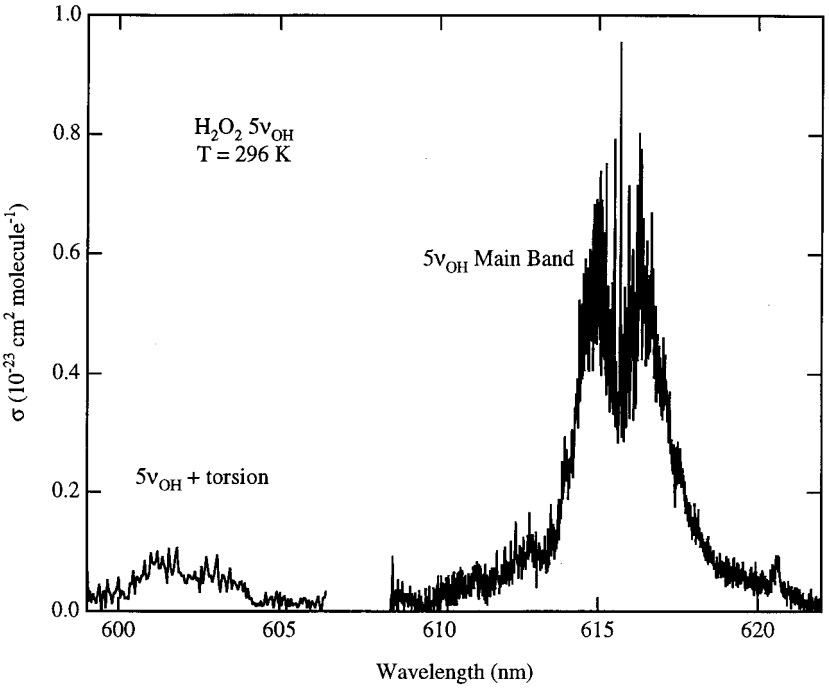

Figure 6. Fourth O−H stretch overtone ($5\nu_{OH}$) spectrum of hydrogen peroxide at room temperature. The band consists of a strong and a weak absorption as in Figure 4. Water overtones contribute less strongly to the signal near the weak absorption than they do in Figure 4.

spectrum that is largely transparent, and it also lies just slightly to shorter wavelength than the $2 \leftarrow 0$ ($b\ ^1\Sigma_g^+ \leftarrow X\ ^3\Sigma_g^-$) transition in O_2.[27] Since the $5\nu_{OH}$ band origin, 16 160 cm^{-1} (618.8 nm),[29] lies 580 cm^{-1} (1.66 kcal mol^{-1}) below the dissociation threshold to OH + NO_2,[30] the DOP mechanism relies on states with sufficient internal energy to dissociate. Thus, DOP is less efficient at lower temperatures. This effect is apparent in the photodissociation experiments of Crim and coworkers,[28,29] who showed that rotational lines at the wings of the nitric acid $5\nu_{OH}$ absorption give rise to single-photon dissociation while those in the center do not. Thus, the transitions that are not present in Figure 5b compared to Figure 5a are precisely those that contribute most significantly to the DOP mechanism.

The rotational structure in the H_2O_2 overtones is significantly more structured. There is less rotational congestion than in the nitric acid overtones, probably because of the larger rotational constants for hydrogen peroxide and the wider overall width of the spectra. Although there are clear features with measurable line widths that extend above the continuum absorption, these are Q branches for different K states ($^{P,R}Q_K$) in this near-prolate symmetric top rather than individual rotational lines. Dübal and Crim[31] have given an excellent discussion of the origin of the rotational and vibrational structure in H_2O_2 overtones. For the purpose of this paper, the important point is that the H_2O_2 overtones have a strong main absorption with a weaker band to shorter wavelength that results from mixing between the O−H stretch and the torsional vibration. The dissociation threshold to produce two OH radicals lies 1150 cm^{-1} (3.29 kcal mol^{-1})[30] above the band origin (16 240 cm^{-1}, 615.8 nm[32]) for the $5\nu_{OH}$ transition, so DOP may occur only from fairly high-lying rotational states. The weak $5\nu_{OH}$ + torsion band lies closer to the dissociation threshold and so is likely to produce OH with a larger quantum yield.[32] Thus, the temperature dependence of the OH quantum yield from DOP will be more pronounced in H_2O_2 than in HNO_3.[10] Figure 4b illustrates the narrowing of the overall absorption bandwidth for the $4\nu_{OH}$ transition. The Q-branch transitions lying closer to the center of the main band are more intense in the low-temperature spectrum. The integrated intensity for $4\nu_{OH}$ reported below comes from the room-temperature spectrum in Figure 4a, but the spectrum in 4b is still useful to illustrate the effect of temperature on the rotational profile.

TABLE 1: Integrated Absorption Cross Sections (cm^2 $molecule^{-1}$ cm^{-1}) for Nitric Acid Overtones

HNO_3	temp, K	$4\nu_{OH}$	$5\nu_{OH}$
this work	296	$(2.25 \pm 0.15) \times 10^{-21}$	$(2.57 \pm 0.24) \times 10^{-22}$
	251	$(2.23 \pm 0.15) \times 10^{-21}$	$(2.41 \pm 0.35) \times 10^{-22}$
estimate, ref 10			1.31×10^{-22}
measurement, ref 11		$(2.37 \pm 0.24) \times 10^{-21}$	
calculation, ref 11		2.17×10^{-21}	2.60×10^{-22}
measurement, ref 14		$(2.8 \pm 1.0) \times 10^{-21}$	

TABLE 2: Integrated Absorption Cross Sections (cm^2 $molecule^{-1}$ cm^{-1}) for Hydrogen Peroxide Overtones

H_2O_2	$4\nu_{OH}$	$5\nu_{OH}$
strong O−H stretch band	$(4.58 \pm 0.39) \times 10^{-21}$	$(5.67 \pm 0.52) \times 10^{-22}$
weak O−H stretch + torsion	$(0.39 \pm 0.10) \times 10^{-21}$	$(0.62 \pm 0.08) \times 10^{-22}$
$T = 253$ K, O−H stretch	$(4.10 \pm 0.65) \times 10^{-21}$	
estimate, ref 10		1.31×10^{-22}
measurement, ref 14	$(4.5 \pm 1.6) \times 10^{-21}$	

Integrated Absorption Cross Sections. Tables1 and 2 present integrated overtone absorption cross sections, and uncertainties and compare them to previously measured, calculated, and estimated values. We carried out the integration numerically using the trapezoid method, which was adequate for the closely spaced points in our data. Contributions to the estimated uncertainties in the tables include the following: uncertainty in the concentration measurement, arising from the cross sections (see above), the flow meter calibrations, and the Zn lamp intensity fluctuations. There is negligible uncertainty in the fitting of individual ring down decay traces; however, slow drift in the empty cavity ring down time due to thermally induced alignment drift can, under worst case conditions, amount to a maximum of 2% and 4% uncertainty in the measured cross sections for the $4\nu_{OH}$ and $5\nu_{OH}$ transitions, respectively. As noted above, there is a small uncertainty associated with the measurement of the ratio L/L_S. For nitric acid there is an additional

uncertainty arising from subtraction of the NO_2 absorption at $5\nu_{OH}$. The integrated absorption cross sections for the weak $4\nu_{OH}$ + torsion band in H_2O_2 includes an estimate of the uncertainty arising from the contribution of water lines, while the $5\nu_{OH}$ + torsion band includes additional uncertainty due to possible baseline drift for this very weak absorption.

Our values for the third overtone ($4\nu_{OH}$) in nitric acid agree to well within the stated uncertainties with the measured value of Donaldson et al.[11] and Zhang et al.[14] At $5\nu_{OH}$, the agreement between our measured value and the calculated value from Donaldson et al.[11] is excellent. The $5\nu_{OH}$ integrated intensity from this work exceeds the estimate used in calculations of atmospheric HO_x production by approximately a factor of 2.[10] Note that Table 1 includes integrated intensities and uncertainties for the low-temperature and room-temperature spectra in Figures 3 and 5, although the room-temperature measurements are more reliable for $5\nu_{OH}$. Both the $4\nu_{OH}$ and $5\nu_{OH}$ integrated absorptions in H_2O_2 are significantly more intense than the corresponding bands in HNO_3. The cross section estimate used by Donaldson et al.[10] to calculate atmospheric OH production from H_2O_2 photolysis at $5\nu_{OH}$ is too low by more than a factor of 4. Thus, they assumed differential cross sections of 10^{-24} cm^2 molecule^{-1} and a bandwidth of 5 nm for each transition to arrive at the integrated cross sections in Tables 1 and 2. The actual scaling between the third and fourth overtones measured in this work is a factor of 8.0 and 8.7, for H_2O_2 and HNO_3, respectively, rather than the factor of 10 predicted by the conventional rule of thumb for overtone intensity scaling.[13]

Donaldson et al.[10] have shown that the calculated enhancement of the atmospheric photolysis rate due to overtone absorption of H_2O_2 and HNO_3 scales linearly with their cross sections. The photolysis rate enhancement is very small for H_2O_2 but more significant for HNO_3. At an altitude of 20 km and a solar zenith angle of approximately 92° (where the actinic flux of red light greatly exceeds that of UV light because of scattering through the longer atmospheric path length), substitution of the cross sections measured in this work for the estimates from Donaldson and co-workers (see Tables 1 and 2) increases the calculated enhancements from approximately 0.5% to 2% for H_2O_2 and from about 15% to 30% for nitric acid.

All of these calculations rest on the assumption that the quantum yield for dissociation of these molecules is unity for absorption to rovibrational states lying above the dissociation threshold. Since it is likely that collisional quenching will compete with dissociation, the quantum yield will not reach unity until the energy is well above threshold. This effect will diminish the HO_x production from overtone absorption in HNO_3 and H_2O_2. Quantifying this effect requires either a measurement of the OH quantum yield as a function of wavelength and temperature, or an accurate calculation of the dissociation rate as a function of energy above threshold.

Measurement of the third overtone cross section for HO_2-NO_2 is currently underway in this laboratory. These results, along with a more detailed discussion of the atmospheric importance of DOP, will appear in a subsequent publication.

Acknowledgment. This work was funded in part by NASA's Upper Atmospheric Research Program. The authors thank Harald Stark for assistance in some of the measurements described in this paper. The authors also thank Hui Zhang, Coleen Roehl, Stan Sander, and Paul Wennberg for communicating their results prior to publication. We thank Greg Frost and John Daniel for several useful discussions.

References and Notes

(1) Levy, H. *Science* **1971**, *173*, 141.
(2) Singh, H. B.; Kanakidou, M.; Crutzen, P. J.; Jacob, D. J. *Nature* **1995**, *378*, 50.
(3) McKeen, S. A.; Gierczak, T.; Burkholder, J. B.; Wennberg, P. O.; Hanisco, T. F.; Keim, E. R.; Gao, R.-S.; Liu, S. C.; Ravishankara, A. R.; Fahey, D. W. *Geophys. Res. Lett.* **1997**, *24*, 3177.
(4) Hanson, D. R.; Ravishankara, A. R. *Geophys. Res. Lett.* **1995**, *22*, 385.
(5) Hanson, D. R.; Ravishankara, A. R.; Lovejoy, E. R. *J. Geophys. Res.* **1996**, *101*, 9063.
(6) Lary, D. J.; Chipperfield, M. P.; Toumi, R.; Lenton, T. *J. Geophys. Res.* **1996**, *101*, 1489.
(7) Salawitch, R. J.; Wofsy, S. C.; Wennberg, P. O.; Cohen, R. C.; Anderson, J. G.; Fahey, D. W.; Gao, R. S.; Keim, E. R.; Woodbridge, E. L.; Stimplfe, R. M.; Koplow, J. P.; Kohn, D. W.; Webster, C. R.; May, R. D.; Pfister, L.; Gottlieb, E. W.; Michelsen, H. A.; Yue, G. K.; Prather, M. J.; Wilson, J. C.; Brock, C. A.; Jonsson, H. H.; Dye, J. E.; Baumgardner, D.; Proffitt, M. H.; Loewenstein, M.; Podolske, J. R.; Elkins, J. W.; Dutton, G. S.; Hintsa, E. J.; Dessler, A. E.; Weinstock, E. M.; Kelly, K. K.; Boering, K. A.; Daube, B. C.; Chan, K. R.; Bowen, S. W. *Geophys. Res. Lett.* **1994**, *21*, 2551.
(8) Wennberg, P. O.; Cohen, R. C.; Stimpfle, R. M.; Koplow, J. P.; Anderson, J. G.; Salawitch, R. J.; Fahey, D. W.; Woodbridge, E. L.; Keim, E. R.; Gao, R. S.; Webster, C. R.; May, R. D.; Toohey, D. W.; Avallone, L. M.; Proffitt, M. H.; Loewenstein, M.; Podolske, J. R.; Chan, K. R.; Wofsy, S. C. *Science* **1994**, *266*, 398.
(9) Wennberg, P. O.; Salawitch, R. J.; Donaldson, D. J.; Hanisco, T. F.; Lanzendorf, E. J.; Perkins, K. K.; Lloyd, S. A.; Vaida, V.; Gao, R. S.; Hintsa, E. J.; Cohen, R. C.; Swartz, W. H.; Kusterer, T. L.; Anderson, D. E. *Geophys. Res. Lett.* **1999**, *26*, 1373.
(10) Donaldson, D. J.; Frost, G. J.; Rosenlof, K. H.; Tuck, A. F.; Vaida, V. *Geophys. Res. Lett.* **1997**, *24*, 2651.
(11) Donaldson, D. J.; Orlando, J. J.; Amann, S.; Tyndall, G. S.; Proos, R. J.; Henry, B. R.; Vaida, V. *J. Phys. Chem. A* **1998**, *102*, 5171.
(12) Phillips, J. A.; Orlando, J. J.; Tyndall, G. S.; Vaida, V. *Chem. Phys. Lett.* **1998**, *296*, 377.
(13) Crim, F. F. *Annu. Rev. Phys. Chem.* **1984**, *35*, 657.
(14) Zhang, H.; Roehl, C. H.; Sander, S. P.; Wennberg, P. O. *Geophys. Res. Lett.*, submitted for publication.
(15) O'Keefe, A.; Deacon, D. A. G. *Rev. Sci. Instrum.* **1988**, *59*, 2544.
(16) Romanini, D.; Lehmann, K. K. *J. Chem. Phys.* **1993**, *99*, 6287.
(17) Scherer, J. J.; Paul, J. B.; O'Keefe, A.; Saykally, R. J. *Chem. Rev.* **1997**, *97*, 25.
(18) Wheeler, M. D.; Newman, S. M.; Orr-Ewing, A. J.; Ashfold, M. N. R. *J. Chem. Soc., Faraday Trans.* **1998**, *94*, 337.
(19) Atkinson, D. B.; Hudgens, J. W. *J. Phys. Chem. A* **1997**, *101*, 3901.
(20) Burkholder, J. B.; Talukdar, R. K.; Ravishankara, A. R.; Soloman, S. *J. Geophys. Res.* **1993**, *98*, 22937.
(21) Brown, S. S.; Talukdar, R. K.; Ravishankara, A. R. *J. Phys. Chem.* **1999**, *103*, 3031.
(22) Vaghjiani, G. L.; Ravishankara, A. R. *J. Geophys. Res.* **1989**, *94*, 3487.
(23) Schneider, W.; Moortgat, G. K.; Tyndall, G. S.; Burrows, J. P. *J. Photochem. Photobiol. A* **1987**, *40*, 195.
(24) Zalicki, P.; Zare, R. N. *J. Chem. Phys.* **1995**, *102*, 2708.
(25) Molina, L. T.; Molina, M. J. *J. Geophys. Res.* **1986**, *91*, 14501.
(26) Burkholder, J. B.; Talukdar, R. K. *Geophys. Res. Lett.* **1994**, *21*, 581.
(27) Rothman, L. S.; Rinsland, C. P.; Goldman, A.; Massie, S. T.; Edwards, D. P.; Flaud, J.-M.; Perrin, A.; Camy-Peyret, C.; Dana, V.; Mandin, J.-Y.; Schroeder, J.; McCann, A.; Gamache, R. R.; Watson, R. B.; Yoshino, K.; Chance, K. V.; Jucks, K. W.; Brown, L. R.; Nemtchinov, V.; Varanasi, R. *J. Quant. Spectrosc. Radiat. Transfer* **1998**, *60*, 665.
(28) Sinha, A.; Vander Wal, R. L.; Crim, F. F. *J. Phys. Chem.* **1989**, *91*, 2929.
(29) Sinha, A.; Vander Wal, R. L.; Crim, F. F. *J. Chem. Phys.* **1990**, *92*, 401−410.
(30) Atkinson, R.; Baulch, D. L.; Cox, R. A.; Hampson, R. F., Jr.; Kerr, J. A.; Rossi, M. J.; Troe, J. *J. Phys. Chem. Ref. Data* **1997**, *26*, 521.
(31) Dübal, H.-R.; Crim, F. F. *J. Phys. Chem.* **1985**, *83*, 3863.
(32) Ticich, T. M.; Rizzo, T. R.; Dübal, H.-R.; Crim, F. F. *J. Chem. Phys.* **1986**, *84*, 1508.